Interference Cancellation in Satcom and Ranging

S. Jayasimha and P. Jyothendar
Signion Systems Ltd., Hyderabad, India
info@signion.com

***Abstract*— Carrier-in-carrier communications, using interference cancellation, can enable bandwidth efficiency, reduced return channel transmit power (via diversity combining) and ranging. In a satellite channel, interference cancellation and diversity combining performance are determined by system bandwidth, orbital delay- and Doppler- adaptation rates, transponder non-linearity and system phase noise, the latter effects being detailed. Interference cancellation can also provide communications and ranging to a co-operating swarm of unmanned aerial vehicles.**

I. INTRODUCTION

Figure 1 shows a carrier-in-carrier communications system, with overlapped (to duplex bandwidth) transmission bands of large aperture hub and a very small aperture terminal (VSAT). At the hub receiver, the VSAT signal's power spectral density (PSD) is usually smaller than the hub signal by approximately the hub-to-VSAT antenna gain ratio. The VSAT signal is demodulated after the hub signal's interference cancellation (IC). Obtained IC is limited by many factors: the hub/ satellite loop's phase noise (PN)[1], transponder non-linearity [1] and frequency and delay tracking rates. The cost of a hub's low-noise block converter depends on its PN mask specification, which, as shown in section 2, is determined by desired IC.

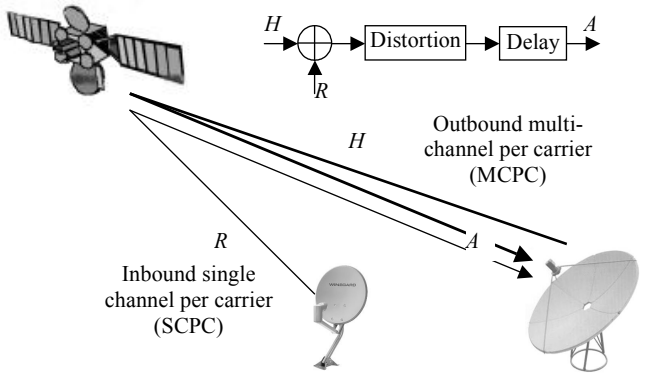

Figure 1: Satellite carrier-in-carrier application

Required battery capacity of an earth (particularly ocean) sensor (to communicate with its hub via satellite) may be reduced by using multiple regional satellites (sensors' broad beam-width transmitters disallowing uplink frequency reuse[2]); hub-based diversity combining (DC) can increase both the satellites' receive antenna aperture and transmit power (e.g., the Tsunami Early Warning System [2] can receive sensor signals via two satellites), the signals' different delays, frequency and phase shifts being compensated prior to DC (Figure 2). Section 3 shows that sensor PN limits diversity gain. Since satellite and hub receivers have more stringent PN masks than the sensor, PN is, with or without DC, the same at the demodulator's input (though the 2-satellite signal-to-noise ratio gain is ~3dB). A demodulator's phase detector computes $\tan^{-1}(Q/I)$, with in-phase (I) and quadrature (Q) matched filter outputs every L symbols [3]; the detector's output PN, the variance sum of system (i.e., the remote up-converter, the satellite transponder, and the hub down-converter) PN, the thermal noise induced PN and PN added by IC or DC, affect demodulator performance. Lower the symbol rate, the greater this PN's influence on demodulator performance [4].

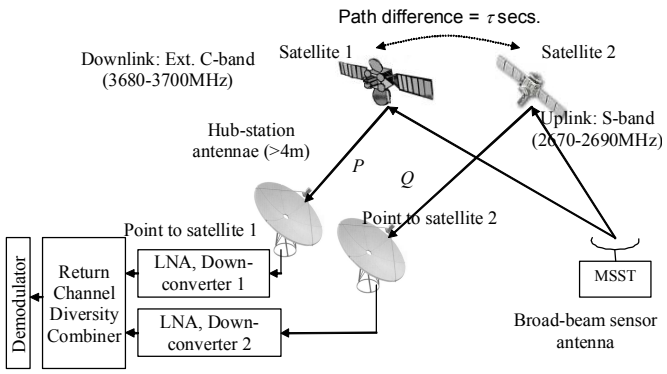

Figure 2: Two-satellite receiver DC

A carrier-in-carrier system, yielding range and Doppler as by-products, allows multiple (severely space-limited) unmanned aerial vehicles (UAVs) integrate ranging, direction-finding and communications, thereby enabling desirable objectives, e.g., de-confliction, collision avoidance and friendly UAV occlusion (by obstacles or target). Section 4 provides details.

II. INTERFERENCE CANCELLATION

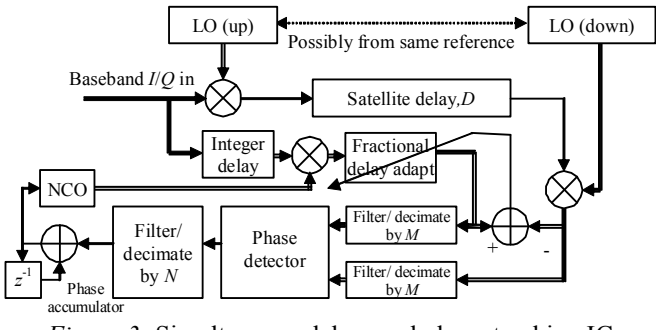

Figure 3: Simultaneous delay- and phase-tracking IC

[1] If an oscillator's output is $V(t)=V_0\cos[\omega_c t+\phi_c(t)]$, with random $\phi_c(t)$ (in radians) and $\phi_c(t)<<1$, $V(t)\approx V_0[\cos(\omega_c t)-\sin(\omega_c t)\cdot\phi_c(t)]$. The oscillator's output is multiplied with $\sin(\omega_c t)$ and low-pass filtered (to reject the double frequency term) to obtain $0.5\cdot V_0[1-\phi_c(t)]$ and the single side-band (SSB) PSD of $\phi_c(t)$ relative to the first term (unity) is the PN spectral power of the oscillator in dBc/Hz.

[2] Multiple sensors simultaneously sharing satellites' bandwidth, e.g., via CDMA, may also use satellite diversity.

Figure 3 shows a carrier-in-carrier's IC, and consists of a phase-locked loop (PLL) and a delay-locked loop (DLL). With zero frequency offset, and the IC's phase corrections disabled, the overall phase detector's output phase variance, $\sigma_{\Delta\theta}^2$, is the sum of the satellite loop's PN variance, the phase error variance due to thermal noise and in-band interference. Without oscillator PN, a PLL $\hat{\theta}(n)=\theta(n)-\sum_{k=1}^{N}h(k)\cdot\hat{\theta}(n-k)$ (B_L is the bandwidth of $H(e^{j\omega})=\sum_{k=1}^{N}h(k)e^{-j\omega k}$ for phase detection rate f_s and $\omega=2\pi f/f_s$,) has phase variance (pg. 128 of [5]), σ_0^2,

$$\sigma_0^2=[(N_0+I_0)B_L/P^2]\cdot[P+(N_0+I_0)B_L] \quad (1)$$

P is signal power, while N_0 and I_0 are noise and interference power spectral densities. A digital phase detector requires complex multiplication and low-pass filtering, followed by 4-quadrant arctangent computation. To minimize computations, the phase detector's input rate is reduced (by low-pass filtering and decimation by M, i.e., a *block phase* estimator) as in Figure 3, possibly (depending on the carrier's spectral occupancy) reducing $P=C/M$ (C is outbound carrier power).

Example: For $E_s/(N_0+I_0)$=-10dB, M=2, post-multiplication filtering/ decimation at minimum signal bandwidth, BW_{min}, N=128, $B_L=BW_{min}/(N\cdot M)$, $P/(N_0+I_0)$=14dB, thermal-noise induced PN is 0.0414 rad^2 (or 0.2035 rad rms). Demodulator performance is unaffected at moderate bit rates as the PN is low-pass. The approximate mean time to cycle slips (pp. 95 of [5]) is (for small closed-loop phase deviations' variance, $\sigma_{\Delta\hat{\theta}}^2$) $[\pi/(2B_L)]\cdot e^{(2\sigma_{\Delta\hat{\theta}}^{-2})}\approx 3\times10^{18}$s (~$3.4\times10^{13}$ days).

A unity dc gain, B_L-bandwidth, loop filter, with closed loop response $(1\text{-}z^{-1})/\{1\text{-}z^{-1}\cdot[H(z)\text{-}1]\}$ and lag ~B_L^{-1}, tracks low-frequency (<B_L) PN and satellite acceleration[3] (high frequency, >B_L, PN remaining unaltered). $\sigma_{\Delta\hat{\theta}}^2$, the IC's output PN is $E[(1-\cos\Delta\hat{\theta})^2+\sin^2\Delta\hat{\theta}]=E[2\cdot(1-\cos\Delta\hat{\theta})]\approx E[\Delta\hat{\theta}^2]=\sigma_{\Delta\hat{\theta}}^2$, i.e., by Parseval's relation, the integral of the PN's PSD > B_L.

Other IC considerations are DLL time resolution (depending on span, L, of a least-mean square adaptive finite impulse response filter, with input sampling rate consistent with cancellation bandwidth[4]) and its noise multiplication (noise variance multiplied by $1+\mu L$ for a unit variance reference, μ being the adaptation step-size [7]). Desired IC determines L, while allowed remote carrier E_b/N_0 degradation (assuming negligible residual outbound carrier) determines μ.. A small μ, while reducing noise multiplication, slows DLL response time - system PN must be less than desired IC at its inverse.

Example: IC of -30dB (0.3dB E_b/N_0 degradation at 64kHz cancellation bandwidth) requires DLL lag (B_L^{-1}) of 125ms (i.e., 8000 samples); consequently, the PN at 8Hz should be -27dBc/Hz (approximating the area beyond 8Hz by the area of a triangle (over-estimating the actual integral); the mask value at 8Hz as per IESS-316 is -40dBc/Hz [8] in Figure 4, while the mask value as per IESS-308 is -28dBc/Hz). As seen by the hub's remote carrier's demodulator, the IC further adds to the satellite loop's PN at low frequencies (<B_L), with diminishing contribution as frequency is increased (as remote terminal's up-converter PN dominates remote-to-hub PN with no IC).

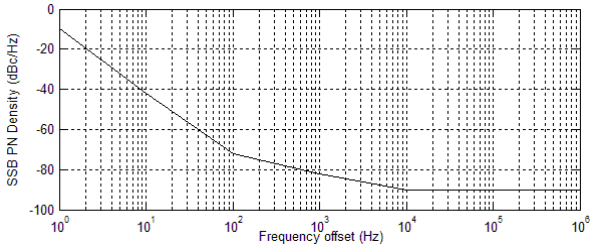

Figure 4: IESS-316 PN mask

In the case of a geostationary satellite, the DLL has a much longer time constant than the PLL (delay rate being small and carrier frequency independent, while Doppler rate increasing linearly with carrier frequency); the two loops don't interact with each other. When a geosynchronous satellite has significant orbital inclination, required Doppler and delay tracking rates are much higher (with maxima at equatorial and high latitudes respectively). This has two consequences:

- Increasing μ to obtain higher DLL tracking rates increases noise multiplication (and hence post-cancellation remote demodulator E_b/N_0 degradation)
- Interacting DLL and PLL increase post-cancellation remote carrier's PN (<B_L) and symbol timing jitter.

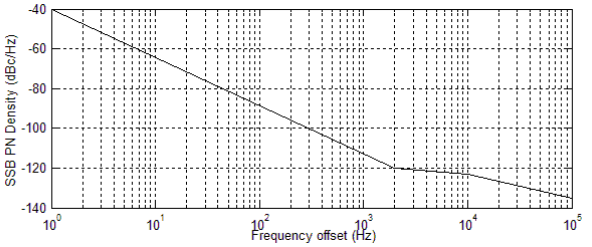

Figure 5: PN mask of sampling clock (here 210MHz)

For a geostationary satellite, the earth-station location and satellite longitude dependent round trip delay, D, is 230-290ms. With both same and different sources (Figure 3's LOs) the reference signal, delayed by D, is time and phase compared (as in Figure 3) with the satellite signal. Therefore, the sampling clock's oscillator PN at $1/D$ must be lower than desired IC. Figure 5 shows a sampling oscillator's PN mask, meeting IC=-30dB at 70 MHz IF and 25MHz bandwidth.

[3] For ±0.1° N-S and E-W station-keeping, a geostationary satellite's maximum earth station relative velocity is 4m/s and maximum (stabilization-dependent) acceleration of 0.075m/s^2 [6], i.e., 20ns/s and 4Hz/s delay and frequency change rate at Ku-band; thus, 2 NCO updates/s at an open loop bandwidth of 2Hz, tracks 4Hz/s. Extreme ranges are $R_{min}=[R_e^2+(R_o+R_e)^2-2R_e(R_o+R_e)\cos(\theta-i)\cos\phi]^{1/2}$ and $R_{max}=[R_e^2+(R_o+R_e)^2-2R_e(R_o+R_e)\cos(\theta+i)\cos\phi]^{1/2}$, θ=latitude of earth station, ϕ=satellite longitudinal shift, i=inclination; delay varies by $2\cdot(R_{max}-R_{min})/c\approx4[R_e(R_o+R_e)\cos\phi\sin\theta\sin i]/\{c\cdot[R_e^2+(R_o+R_e)^2]^{1/2}\}$ (=127μs for i=0.1°, θ=60°, ϕ=0°, R_o=35,786km and R_e=6,378km).

[4] An L-tap DLL converges to a windowed sinc[$\alpha(n\text{-}D)$], α being the signal's spectral occupancy. L is such that windowing power loss is less than desired IC (e.g., IC=-35dB, α=1/5, L~45); given L, smaller α degrades IC (also, the signal's autocorrelation matrix's eigenvalue spread, i.e., $\lambda_{max}/\lambda_{min}$, increases, slowing convergence [7]).

III. DIVERSITY COMBINING

A small aperture terminal, with small angular attenuation over inter-satellite spacing, may utilize adjacent satellites bandwidth to provide a stronger hub[5] demodulator signal (Figure 6, a weighted addition augmentation of Figure 3's IC). The hub's receive antennas have high directivity (so that they each obtain the spatially separated transponder signals).

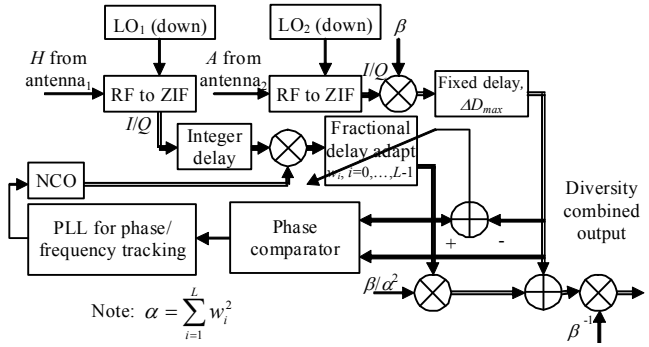

Figure 6: 2-channel (satellites/ hub antennas) MRRC

The range R of a geostationary satellite from an earth station at latitude, θ, and longitudinal shift (from satellite longitude), ϕ, is $R=[R_e^2+(R_o+R_e)^2-2R_e\cdot(R_o+R_e)\cdot\cos\theta\cos\phi]^{1/2}$, R_o=35,786km and R_e=6,378km [6]. For two satellites' angular separation of (small, typically 2-3°) $\Delta\phi$, the range difference between hub and satellites $\Delta R\approx 2[R_e(R_o+R_e)\sin\phi\sin\Delta\phi\cos\theta]/[R_e^2+(R_o+R_e)^2]^{1/2}$, and is maximized when an equatorial earth station has large ϕ (not the best choice as ϕ=0 maximizes coverage area). The sensor-to-hub range difference, the sum of sensor-to satellite and satellite-to-hub range differences, is maximized when both sensor and hub have the same longitude direction (say ϕ_s and ϕ_h respectively and for farthest sensors, $\phi_s>\phi_h$) relative to the satellite. *Example:* for equatorial sensor and earth station with ϕ_s=30°, ϕ_h=15° and $\Delta\phi$=3°, range differences[6] are 330 and 171km (1.7ms differential delay).

By design, the two hub receive antennas can have identical apertures; each received signal's strength is sensor location (i.e., relative ratio being the inverse square of the distances to the two satellites) and fading dependent. For two C-band geostationary transponders, this ratio is close to unity (unless the footprints are very different). For equal receivers' noise variances, Figure 6's maximal-ratio receive combining (MRRC) is optimum. Challenges for DC (vis-à-vis IC) are:

- The remote terminal's up-converter's PN is system PN.
- System bandwidths are typically small (of the order of 0.6-20kHz) because of:
  - Many distributed sensors in the satellite's footprint
  - Limited remote terminal transmit power

The delay locked loop's lag is reduced (i.e., by increasing μ and decreasing L), compromising diversity gain.

Example: Figure 7(a) shows a low-cost up-converter's PN mask. With 0.1s delay-lock loop time-constant, IC is -17dB (noise multiplication and delay-locked loop time constant being inversely related). Separately, B_L=10Hz limits IC to -20dB. With both contributions, IC is -16dB. As predicted, Figure 7(b) has 2.6dB two-satellite MRRC gain (BPSK at 64 ksymb/s). In addition, the ratio of combined signal power to PN variance below 10Hz also decreases by 0.4dB (for B_L loop filter, the 2 PNs sum coherently below B_L, but not above B_L).

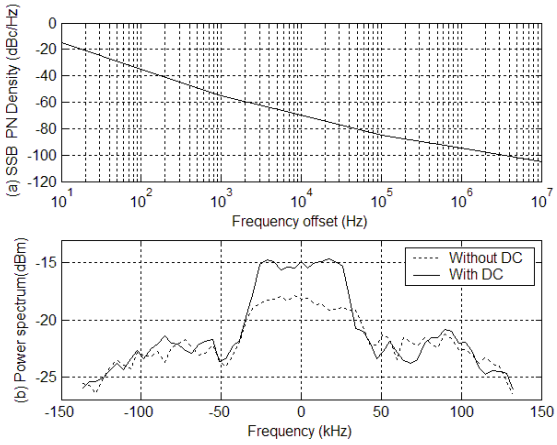

Figure 7: DC gain (b) with low-cost up-converter's PN (a)

IV. AIRBORNE KINEMATIC POSITIONING FOR UAVS

Using the Global Positioning System (GPS), precise airborne positioning via carrier phase measurements has difficulties of:

- Disambiguation
- Cycle slip repair
- Interpolating GPS fixes using inertial navigation

UAVs using low-cost, noisy, surface micro-machined MEMS inertial sensors have significant position and velocity errors. In addition, integrating autonomous target acquisition and bearing-based pursuit[7] (e.g., phased-array radar in the UAV's nose), is challenging in terms of operating frequency, electronics packaging and cost. Instead, cooperating entities' radio proximity detection (RPD) allows bearing inference.

[5] When adjacent satellites have different polarizations and the reduced aperture (e.g., maritime) VSAT's reflector antenna (with bore-sight bisecting the satellites) has receivers at both polarizations [9], forward channel space-polarization-time coding may be used.

[6] Rapid ionospheric changes at dusk (when total electron content, TEC, drops) induces range differential range $\Delta s=\pm 40.31\cdot\Delta TEC/f^2$ m [10], where f is frequency and ΔTEC=differential TEC in $1m^3$ (TEC varies from 1×10^{16} at night to 5×10^{17} at daytime) over the angular inter-satellite separation. Although differential delay uncertainty becomes significant at a sufficiently high symbol rate (or at a low enough carrier frequency), it is negligible at the symbol rate and carrier frequency used in this (sensor data collection) application.

[7] Rate-using true proportional navigation guidance [11] may apply (augmented by inter-communicated periodic GPS fixes). Our inherently secure (the target can't separate the two signals without a reference), low probability of intercept (LPI) and anti-jam (AJ) communications method also provides low latency range and Doppler data. Lower the carrier frequency, the smaller the Doppler tracking rate; [12] uses 902-928MHz, which, with 2 carriers, has <3m range resolution, and required Doppler acquisition and tracking of ±2,500Hz (accounting for oscillator offsets and drift) and ±300Hz/s at 700m/s speed and $100m/s^2$ acceleration respectively. Short-range (<2km) acquisition, at the signal's sampling rate, suffices in this case (unlike in satellite IC).

Figure 8's "paired-carrier"[8] RPDs are (i) coordinated UAV pair and (ii) star-coordinated UAVs (using either several paired-carriers or CDMA on a single carrier pair).

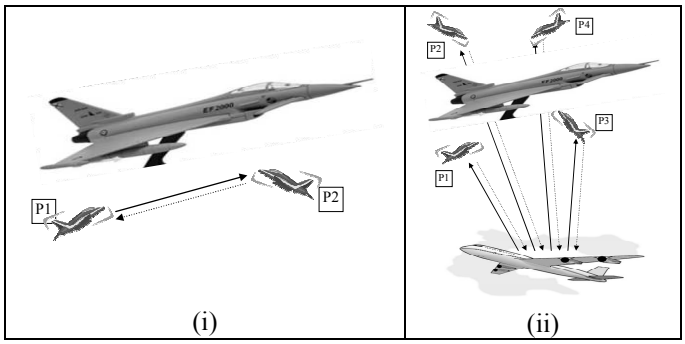

Figure 8: (i) Co-ordinated UAV pair and (ii) UAV swarm

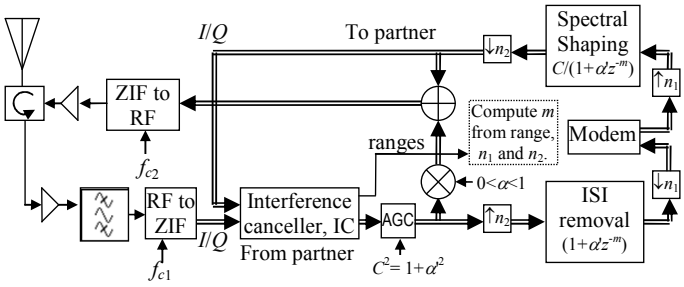

Figure 9: UAV's transceiver[9]; IC cancels all lagged CSs.

In case (i), communication[10] with a partner UAV (each transmitting a different carrier as in Figure 9, with modulator output and α-scaled post-IC received signal termed as communications, CS, and ranging, RS, signals) exploits range and Doppler information inherent in carrier-in-carrier IC. As the target nears, three RS's[11] correlate at range lags[12] (in addition to transponder processing lag) of:

- Twice the inter-UAV range; receiver power $\propto \alpha^2/(4\pi \cdot AB^2)$
- The perimeter of the triangle formed by the two UAVs and the target (whose bi-static radar cross section, RCS, denoted by σ); power $\propto 2\alpha^2\sigma/[(4\pi \cdot AT \cdot BT)^2]$ (1-13 of [14], with two ways[13] of constructing the triangle and $f_{c1} \approx f_{c2}$, $\sigma >> \lambda^2 = c \cdot f_c^{-1}$).
- Twice the UAVs to target ranges' sum; power $\propto \alpha^2 \cdot AB^2 \cdot \sigma^2 / [(4\pi)^3 (AT \cdot BT)^4]$

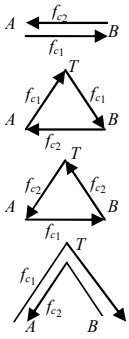

Practically, only the first two signals' ICs are relevant and the second return to CS power ratio, $2\alpha^2\sigma(AB)^2/[4\pi(AT \cdot BT)^2]$, sets required IC, (designed to be $>K$, for reliable acquisition).

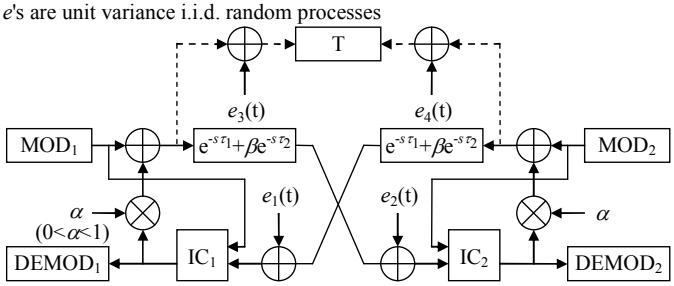

Figure 10: UAV signals' flow graph (no frequency offsets[14])

Figure 10 shows the two UAVs transponders' un-cancelled noise (including jamming and un-cancelled clutter, neglecting CS target path) feedback, including target returns (for LPI analysis, dashed lines showing target's receptions at f_1 and f_2). With fixed delays, noise (as well as un-cancelled signal) amplification (Figure 11) occurs. The input noise spectrum at the left demodulator, $G(s)$, is:

$$G(s) = \frac{\left(1+\beta-\alpha\beta e^{-2s\tau_1}-\alpha e^{-2s\tau_2}\right)\left[E_1(s)+\alpha E_2(s)\right]}{\left(1-\alpha e^{-2s\tau_1}\right)\cdot\left(1-\alpha e^{-2s\tau_2}\right)} \qquad (2)$$

The pass-band noise power gain ($\geq 1 \forall \omega$) is:

$$G(\omega,\alpha,\beta,\tau_1,\tau_2) = \frac{\left|1+\beta-\alpha\beta e^{-2j\omega\tau_1}-\alpha e^{-2j\omega\tau_2}\right|^2\left(1+\alpha^2\right)}{\left|1-\alpha e^{-2j\omega\tau_1}\right|^2\cdot\left|1-\alpha e^{-2j\omega\tau_2}\right|^2} \qquad (3)$$

$$\overline{G} = G(\alpha,\beta,\tau_1,\tau_2) = \frac{1}{2\pi F_P}\int_0^{2\pi F_P} G(\omega)d\omega \qquad (4)$$

Here, F_P=LCM($\frac{1}{2}\tau_1^{-1}$, $\frac{1}{2}\tau_2^{-1}$)Hz, ω is angular frequency and β is target scattering relative to the direct inter-UAV signal. The ratio of UAV-to-target demodulators' signal-to-noise ratios is $\{1+[\alpha^2 S/G(\alpha,\beta,\tau_1,\tau_2)]\}$; thus, the LPI optimum α is:

$$\alpha_{LPI} = 2G(\alpha,\beta,\tau_1,\tau_2)/[\partial G(\alpha,\beta,\tau_1,\tau_2)/\partial\alpha] \qquad (5)$$

---

[8] Continuous (rather than pulsed) waveform and a single transmit/ receive (T/R) antenna (rather than spatially isolated T/R antennas).

[9] Low-power, small-footprint, COTS devices spanning 0.8-2.7GHz convert from (to) radio frequency (RF) to (from) zero-IF (ZIF).

[10] Communication signals, with low autocorrelation at non-zero lags (from 0 to 3 times the maximum range lag), modulations may have different discrete amplitude levels [13].

[11] Assumes slowly-varying target [14] (where return's amplitude/ Doppler can be tracked) and ignores clutter (assumes high-altitude).

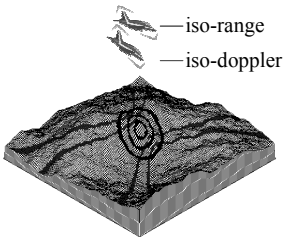

Only distant ranges (relative to the target) are received when antenna pattern has high attenuation in a cone about the UAV's downward vertical axis. For typical clutter, the bi-static iso-ranges are incoherent and iso-dopplers time-dispersed. Hence, clutter is modeled as noise (signal being a nearer compact target).

Different UAV's transmit/ receive frequencies ensure that only the other UAV's transponder (*not* its RCS) provide inter-UAV range.

[12] Drawbacks of a system without IC (i.e., 2 carriers for A's communication and B's ranging transponder and, vice-versa, 2 more carriers), besides doubling bandwidth, are:

- The target correlates A's modulator and B's transponder signals to passively obtain (ignoring UAV RCS) lags corresponding to a) AB+BT-AT (early) and b) 2·BT (late). From B's modulator and A's transponder signals, it also finds AT, whence AB. It can then adjust jamming power to disrupt communications/ ranging.
- Encryption required to secure the communication links

[13] In general, when $\sigma >> c/f_c$, received power doubles (the numerous target scattering returns' vector sum constituting σ, excepting for specular returns, where paths' phase shift is $[f_{c1}-f_{c2}]\cdot[AT+BT-AB]/c$).

[14] As in the analogous speakerphone application, introduced frequency offsets may reduce noise resonance magnitude [15].

From an AJ standpoint, α gets upper bounded by the IC's PLL phase variance limit (a +ive K), i.e., solving (5.3-25 of [5])

$$[(G_0N_0+I_0)B_L/(\alpha_C{}^4P^2)]\cdot[\alpha_C{}^2P+(G_0N_0+I_0)B_L]\leq K \qquad (6)$$

P and I_0 are CS power and spectral density respectively, N_0 the jammer plus noise spectral density, B_L the PLL's loop bandwidth and $G_0=G(0,\alpha,\beta,\tau_1,\tau_2)$. Using the smaller of α_C and α_{LPI}, a minimum IC dynamic range is imposed. This RS/ CS system's required E_b/N_0 increases by $(1+\overline{G})$ (compared to just a CS), but benefits are LPI, AJ and spectral efficiency.

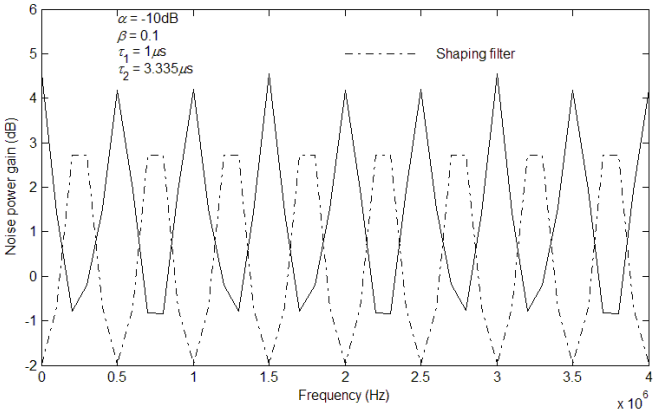

Figure 11: Example noise power gain spectrum

Kinematic-induced frequency offset does not reduce noise power (e.g., for f_c≈900MHz, 100m/s relative velocity, frequency de-coherence is 300Hz; with 300m inter-UAV distance, phase de-coherence is just 0.024°). Though regenerative transponders avoids noise feedback, they add to demodulation/ decoding delay, in turn, requiring more stringent phase noise and low-jitter symbol timing recovery. On the other hand, the target can passively find the sum of its ranges to the UAVs, as well as the range between them, by spectral analysis (Figure 11). Range-LPI (while [16]'s dirty-paper encoding's objective and assumptions are different, its "imprecise" title is nonetheless evocative) adapts[15] coding and modulation shape to UAV /target ranges, inverts partial-response at demodulator input and then decodes decision variables; when acquiring range (sweeping over B_L, in pp. 143 of [5]), unshaped modulator power is temporarily increased.

As antenna beam-widths are broad[16] (and bearing information unavailable), target position is ambiguous[17] to an ellipsoid (for an interceptor-pair at the two foci); Measuring range and Doppler with varying inter-foci distance, or major-axis orientation, or both, may aid disambiguation and pursuit; though beyond this paper's scope, the interceptors, during pursuit, could execute several pre-synchronized, seemingly random, ellipsoid re-orienting maneuvers (Figure 12).

[15] If modulator output and IC output sample rates are in a ratio n_1/n_2, $G(z)[1+\alpha' z^{-m}]^{-1}$ is a high-resolution shaper (for $\beta<<\alpha<<1$), with $(1+\alpha' z^{-m})\cdot G(z)$ inverting receiver partial-response, where $\alpha'=\alpha/\gamma$, γ=receiver SNR and $G(z)$ an interpolator.

[16] [12]'s 1W communication antenna, a ¼ wave radiator on ¼ wave radius (8.22cm^2) ground-plane, mounts on the fuselage's top aft.

[17] The last lag (of the three) is redundant (determined from the first two); disambiguation requires side information (e.g., a maneuver).

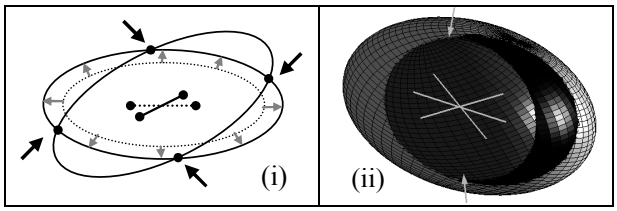

Figure 12: 2 UAVs' disambiguation by major axis rotations (i) 2-D (ii) 3-D; arrows show possible target locations

V. CONCLUSION

Conventional IC and DC systems are performance limited by system PN and these limits are derived. Ranging, inherent to IC, may also aid direction-finding and pursuit (with application to UAV swarming).

REFERENCES

[1] S. Jayasimha and P. Jyothendar, "Canceling Echoes distorted by Satellite Transponders," Proc. of *Natl. Conf. on Comm. (NCC-2006)* pp. 112-116, Omega Scientific Publishers, New Delhi, ISBN 81-85399-80-8.

[2] www.incois.gov.in/documents/Final Presentation for Press Meet Dec 26, 2006.pdf (accessed: 3-12-2007)

[3] C.G. Hiremath and S. Jayasimha, "Design of burst-mode decision-feedback QPSK demodulator," Proc. of *SPCOM '99*, pp. 81-85.

[4] S. Jayasimha, T. Praveen Kumar and P. Jyothendar, "DPLL adaptation and I/Q imbalance compensation for mobile satellite demodulators," Proc. of *Natl. Conf. on Comm. (NCC-2007)* pp. 245-256, Solar Press, Kanpur, ISBN 81-904444-0-8.

[5] J.K. Holmes, "Coherent Spread Spectrum Systems," Krieger Pub Co., ISBN: 0894644688, chapters 4 and 5.

[6] W.L. Pritchard, H.G. Suyderhoud and R. A. Nelson, *Satellite Communication Systems Engineering*, Prentice Hall, NJ, pp. 62-80, pp. 98-104 and pp. 125-131.

[7] B. Widrow and S.D. Stearns, *Adaptive Signal Processing*, Prentice Hall, Upper Saddle River, NJ, 1985.

[8] *Intelsat Earth Station Standards* (IESS), Document IESS-316, October 24, 2003.

[9] I. Frigyes and P. Horváth, "Polarization-Time Coding in Satellite Links", IEEE-SSC newsletter, May 2005.

[10] B.W. Parkinson and J.J. Spilker, *Global Positioning System: Theory & Applications,* Vol. 1, Jan., 1996**.**

[11] N.A. Shneydor, *Missile guidance and pursuit*, Horwood, Chichester, UK, 1998, pp. 109, ISBN-10: 1898563438.

[12] www.cloudcaptech.com/download/piccolo/piccolo system software/version 2.0.4/docs/piccolo vehicle integration guide.pdf (accessed: 3-12-2007)

[13] P. Moulin, "Signal Transmission with Known Interference Cancellation" *IEEE Signal Processing Magazine*, January 2007, pp. 134-136.

[14] J.L. Eaves and E.K. Reedy, *Principles of Modern Radar*, Van Nostrand Reinhold Company, New York, 1987.

[15] M.R. Schroeder, "Improvement of Acoustic-Feedback Stability by Frequency Shifting", J. Acoust. Soc. Am., vol. 36, no. 9, pp. 1718-1724, 1964.

[16] M. Costa, "Writing on dirty paper," *IEEE Trans. Inf. Theory*, vol. 29, no. 3, pp. 439-441, May 1983.